INTERNATIONAL JOURNAL FOR NUMERICAL METHODS IN FLUIDS, VOL. 25, 1003–1023 (1997)

HYBRIDIZATION BETWEEN σ- AND z-CO-ORDINATES FOR IMPROVING THE INTERNAL PRESSURE GRADIENT CALCULATION IN MARINE MODELS WITH STEEP BOTTOM SLOPES

HANS BURCHARD[1]* AND OLE PETERSEN[1,2]

[1] *International Research Centre for Computational Hydrodynamics, ICCH, Danish Hydraulic Institute, Agern Allé 5, DK-2970 Hørsholm, Denmark*

[2] *Department of Civil Engineering, Aalborg University, Sohngaardsholmsvej 57, DK-9000 Aalborg, Denmark*

SUMMARY

It is discussed in this paper how the pressure gradient error in general vertical co-ordinate models (in which the σ-transformation is a special case) can be reduced by means of hybrid models. For a better understanding, the derivation of such a general vertical co-ordinate model from the Cartesian co-ordinate model is given. Two types of hybridization between σ- and z-co-ordinate models, each using one parameter specifying the degree of hydridization, are presented: (i) the mixed layer transformation with a constant number of layers which are refined near the surface and (ii) the z/σ-transformation which introduces steps near the bottom. In order to achieve good results with the models using other than σ-co-ordinates, a profile-conserving momentum advection discretization is developed. The different co-ordinate transformations are tested with 2D barotropic and baroclinic flows over a topographic bump. Those models with nearly horizontal co-ordinate surfaces in the stratified area give the best correspondence with an isopycnal reference solution. © 1997 John Wiley & Sons, Ltd.

Int. J. Numer. Meth. Fluids, **25**: 1003–1023 (1997)

No. of Figures: 8. No. of Tables: 2. No. of References: 20.

KEY WORDS: 3D modelling systems; general vertical co-ordinates; pressure gradient; hydrostatic consistency; momentum advection

1. INTRODUCTION

In recent years an intensive and often controversial discussion has arisen about the so-called pressure gradient problem in hydrostatic geophysical models with terrain-following vertical co-ordinates. Haney[1] brought the discussion from the meteorological into the oceanographic community. Expressed in terms of general vertical co-ordinates, the internal, buoyancy-driven horizontal pressure gradient term consists of two parts, the buoyancy gradient along the co-ordinate surfaces and the vertical buoyancy gradient multiplied by the co-ordinate slope. These two terms analytically cancel out when the buoyancy distribution is horizontally homogeneous. In the discrete space this is

* Correspondence to: H. Burchard, Joint Research Centre, Space Applications Institute, TP 690, I-21020 Ispra (VA), Italy.

Contract grant sponsor: Danish Research Foundation.

CCC 0271–2091/97/091003–21 $17.50 *Received July 1996*

generally not the case and leads to truncation errors. A simple local criterion for the reliability of the internal pressure gradient calculation is the so-called 'hydrostatic consistency condition'.[1] A grid is locally hydrostatically inconsistent if the co-ordinate slope exceeds the ratio of vertical to horizontal discretization. Assuming that the vertical buoyancy distribution can be described by a polynomial, Beckmann and Haidvogel[2] showed in an extensive analysis that the pressure gradient error depends on the co-ordinate slope, the slope of the isopycnals and the polynomial degree of the vertical buoyancy distribution.

There are basically two possible approaches for improving the pressure gradient calculation in general vertical co-ordinates: developing new discretization techniques for the internal pressure gradient or providing vertical co-ordinate transformations with certain advantages.

The first is certainly limited by the findings of Beckmann and Haidvogel[2] mentioned above. However, different approaches have been presented. McCalpin[3] got improved results by implementing a fourth-order rather than a second-order discretization of the horizontal, along co-ordinate gradients, while using a spectral approach in the vertical. Some papers suggest calculating the pressure gradient term in z-co-ordinates. This leads to the vertical interpolation of buoyancy values in order to compute the horizontal gradients. Beckmann and Haidvogel[2] mention problems connected with the necessary extrapolations at the bottom when the topography is steep. Stelling and van Kester[4] suggested a non-linear interpolation. They use the same computational stencils for the discretization of the internal pressure gradient and the horizontal diffusion of concentrations. By doing this, they construct a discrete diffusion operator which is monotone, a property which is difficult to obtain in generalized vertical co-ordinates. Test calculations show on the other hand that pressure gradient forces are generally underpredicted with this method,[5] leading to errors of the order of the σ-co-ordinate error.

There are two co-ordinate transformations which avoid the pressure gradient problem, because then one of the two balancing terms vanishes. The along co-ordinate gradient term vanishes, when the isopycnal transformation is carried out, where the surfaces of constant velocity are identical with the co-ordinate surfaces. This transformation is only defined at vertical lines where the stratification is stable and therefore does not apply to typical mixing or convection situations. This is why most of the isopychal models are coupled with a mixed layer model for the upper ocean (see e.g. Reference 6).

The second part of the pressure gradient term vanishes if the co-ordinate surfaces are horizontal. This is the case for z-co-ordinate models (see e.g. References 7 and 8). The problems of these models are mainly connected with the flow along a sloping bottom and the surface (for small-scale applications including tides, see References 9 and 10.

Apart from the pressure gradient problem, terrain-following co-ordinates, for which the linear σ-transformation is the best known, have some significant advantages compared with z-co-ordinates. These are mainly the easy treatment of the kinematic boundary conditions at the bottom and surface and the high resolution in the shallower part of the domain.

Hybridizing between σ-co-ordinates and either z- or isopycnal co-ordinates would allow for optimizing the model performance by combining the advantages of the different co-ordinate systems. In order to achieve that, Deleersnijder and Ruddick[11] presented a formulation for marine models with an arbitrary vertical co-ordinate transformation. Implementing this general type of co-ordinate in a numerical model allows in principle for arbitrary layer distributions in each time step.

Different approaches for hydridization techniques have been suggested in the past. An interpolation between σ- and isopycnal co-ordinates could be achieved by introducing arbitrary Lagrangian–Eulerian (ALE) co-ordinates[12] in the vertical. With this approach, vertical co-ordinates are in principle treated in a Lagrangian way, i.e. moved with the vertical flow, and afterwards rezoned to a layer distribution which is advantageous for the specific application. This is promising but difficult, because the grid depends on the internal structure of the flow. The task is to find general

rules for rezoning the co-ordinate surfaces if the stratification is weak or unstable or if mixing processes take place. A model which in principle has adopted this approach is the layered ocean model of Jensen.[13]

More work has been done on the hybridization between σ- and z-co-ordinates. Beckers[14] introduced one fixed z-level into his model and distributed σ-layers between bottom and z-level and between z-level and surface respectively. By means of this a zero co-ordinate slope (for zero surface slope) in the stratified region above the z-level is achieved. A more general approach was chosen by Gerdes.[15] Assuming a given z-level distribution, a hybridization technique is presented where the co-ordinates coincide with the z-level at maximum water depth and with σ-layers at minimum water depth. By means of this, co-ordinate surfaces with small slopes are concentrated in the stratified region near the surface.

The scope of this paper is to show how co-ordinate transformations hybridizing between σ- and z-c-ordinates can considerably improve baroclinic flow simulations on coastal and estuarine scales compared with pure σ-co-ordinate models. After presenting the mathematical model in Cartesian co-ordinates (Section 2) and deriving the transformed equations from it (Section 3), the layer integration is performed as a first step of discretization (Section 4).

Special numerical problems of general vertical co-ordinates are discussed in Section 5. It is shown in Section 5.1 that the momentum-conserving discretization of the horizontal advection (the advection along constant co-ordinate surfaces will simply be referred to as 'horizontal advection' in this paper) introduces artificial shear for all co-ordinate transformations except the σ-transformation. This is especially true for z-co-ordinates. A 'profile-conserving' momentum advection discretization including the discrete continuity equation will be presented. In Section 5.2 the horizontal buoyancy discretization is discussed. It is shown that the violation of the hydrostatic consistency condition has the consequence that the pressure gradient calculation is based on extrapolations rather than interpolations of discrete values. Apart from the advection and pressure gradient discretization, other problems such as horizontal or isopycnal diffusion or Coriolis acceleration will not be discussed in this paper.

Two different techniques are presented in Section 6, where a single parameter determines the degree of hybridization. Both include σ-co-ordinates and horizontal co-ordinates as special cases. The first approach, which is similar to Gerdes' transformation,[15] is based on a constant number of vertical layers. It may be called the 'mixed layer transformation' because of the concentration of co-ordinate levels near the surface mixed layer. The second transformation introduces a z/σ-type co-ordinate with steps near the bottom and allows the grid to adjust to a moving surface.

The performance of the profile-conserving momentum advection and the two transformations will be tested in Section 7 for coastal applications in 2D barotropic and baroclinic flows over a topographic bump.

2. HYDROSTATIC MODEL IN CARTESIAN CO-ORDINATES

The co-ordinates that span the Cartesian space will be denoted as (t^*, x^*, y^*, z); derivatives along these co-ordinates will be marked by asterisks. Neglecting horizontal diffusion, the flux form of the momentum equations for modelling geophysical ocean and coastal dynamics reads in these co-ordinates as

$$\partial_t^* u + \partial_x^*(u^2) + \partial_y^*(uv) + \partial_z^*(uw) - \partial_z^*(v_t \partial_z^* u) - fv = -\frac{1}{\rho_0}\partial_x^* p, \tag{1}$$

$$\partial_t^* v + \partial_x^*(vu) + \partial_y^*(v^2) + \partial_z^*(vw) - \partial_z^*(v_t \partial_z^* v) + fu = -\frac{1}{\rho_0}\partial_y^* p. \tag{2}$$

Here u, v and w are the velocity components with respect to the x-, y- and z-direction respectively, the vertical co-ordinate z ranges from the bottom $-H(x, y)$ to the surface $\zeta(t, x, y)$, ν_t is the vertical eddy viscosity, f is the Coriolis parameter, ρ is the density, ρ_0 is a constant reference density and p is the pressure. Assuming the pressure to be hydrostatic, i.e.

$$\partial_z p + g\rho = 0, \tag{3}$$

the pressure gradient in equation (1) can be expressed as

$$-\frac{1}{\rho_0}\partial_x^* p = -g\frac{\rho(\zeta)}{\rho_0}\partial_x^*\zeta + \int_z^\zeta \partial_x^* b \, \mathrm{d}z', \tag{4}$$

with the buoyancy

$$b = -g\frac{\rho - \rho_0}{\rho_0}. \tag{5}$$

In equation (4) the first term on the right-hand side is called the external and the second the internal pressure gradient force.

By means of integrating the continuity equation

$$\partial_x^* u + \partial_y^* v + \partial_z^* w = 0 \tag{6}$$

under consideration of the kinematic boundary conditions

$$w = -u\partial_x^* H - v\partial_y^* H, \quad z = -H, \tag{7}$$

$$w = \partial_t^*\zeta + u\partial_x^*\zeta + v\partial_y^*\zeta, \quad z = \zeta, \tag{8}$$

the surface elevation equation can be derived as

$$\partial_t^*\zeta = -\partial_x^*\int_{-H}^{\zeta} u \, \mathrm{d}z - \partial_y^*\int_{-H}^{\zeta} v \, \mathrm{d}z. \tag{9}$$

The equation for a concentration, which can e.g. represent temperature or salinity, is given by

$$\partial_t^* c + \partial_x^*(uc) + \partial_y^*(vc) + \partial_z^*(wc) = 0. \tag{10}$$

Diffusion of concentrations will not be considered in this paper. The coupling between the concentration equation and the momentum equations is due to an algebraic equation of state:

$$\rho = \rho(c). \tag{11}$$

3. HYDROSTATIC MODEL IN GENERAL VERTICAL CO-ORDINATES

A vertical co-ordinate transformation γ (see e.g. Reference 11) will be applied which maps the physical space into a transformed space spanned by the co-ordinates (t, x, y, γ) (see Figure 1). Here γ is assumed to be monotone with respect to z, i.e.

$$\gamma = \gamma(t^*, x^*, y^*, z) \quad \Leftrightarrow \quad z = z(t, x, y, \gamma). \tag{12}$$

Derivatives in the transformed space will be denoted by ∂_t, ∂_x, ∂_y and ∂_γ. The values for γ at the bottom and top are constant in time and space so that the approach shown here provides boundary-fitted co-ordinates in the vertical. Here

$$\gamma(\zeta) = 0, \qquad \gamma(-H) = -1 \tag{13}$$

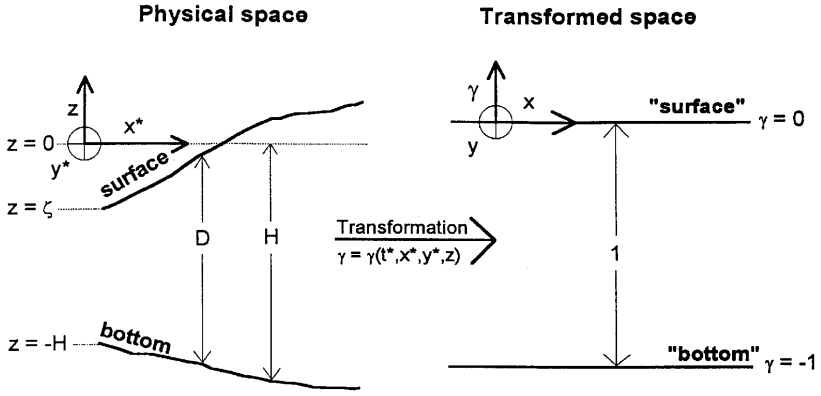

Figure 1. Sketch of principle of vertical co-ordinate transformation (adapted from Reference 11)

are used. The so-called Jacobian of the transformation,

$$J := \partial_\gamma z = (\partial_z^* \gamma)^{-1}, \tag{14}$$

plays a central role in the transformation of the equations. It can easily be seen from (13) and (14) that

$$\int_{-1}^{0} J \, \mathrm{d}\gamma = \zeta + H = D, \tag{15}$$

where D is the water depth.

Derivatives and integrals of a function f in γ-co-ordinates read as

$$\partial_z^* f = \frac{1}{J} \partial_\gamma f, \tag{16}$$

$$\partial_x^* f = \partial_x f + \partial_x^* \gamma \partial_\gamma f, \tag{17}$$

$$\partial_t^* f = \partial_t f + \partial_t^* \gamma \partial_\gamma f, \tag{18}$$

$$\int_a^b f(z) \, \mathrm{d}z = \int_{\gamma(a)}^{\gamma(b)} J(\gamma') f(\gamma') \, \mathrm{d}\gamma'. \tag{19}$$

The following relations can be derived from (17) and (18):

$$\partial_x^* \gamma = -\partial_x z J^{-1}, \qquad \partial_t^* \gamma = -\partial_t z J^{-1}, \tag{20}$$

$$\partial_x J = -\partial_\gamma (J \partial_x^* \gamma), \qquad \partial_t J = -\partial_\gamma (J \partial_t^* \gamma). \tag{21}$$

A new definition of the vertical velocity simplifies the transformation of the equations:

$$\tilde{\omega} = d_t^* \gamma = \partial_t^* \gamma + u \partial_x^* \gamma + v \partial_y^* \gamma + w \partial_z^* \gamma \quad \Leftrightarrow \quad w = J(\tilde{\omega} - \partial_t^* \gamma - u \partial_x^* \gamma - v \partial_y^* \gamma), \tag{22}$$

where d_t^* denotes the substantial derivative in the physical space. Now the continuity equation (6) can be transformed to the γ-co-ordinate with the aid of (20)–(22):

$$\partial_t J + \partial_x (Ju) + \partial_y (Jv) + \partial_\gamma (J\tilde{\omega}) = 0. \tag{23}$$

The momentum equations can now be written as

$$\partial_t(Ju) + \partial_x(Ju^2) + \partial_y(Juv) + \partial_\gamma(\tilde{\omega}Ju) - \partial_\gamma\left(\frac{\nu_t}{J}\partial_\gamma u\right) - fJv = -J\frac{\partial_x^* p}{\rho_0}, \tag{24}$$

$$\partial_t(Jv) + \partial_x(Jvu^2) + \partial_y(Jv^2) + \partial_\gamma(\tilde{\omega}Jv) - \partial_\gamma\left(\frac{\nu_t}{J}\partial_\gamma v\right) - fJu = -J\frac{\partial_y^* p}{\rho_0}, \tag{25}$$

where the pressure term (4) in the x-direction can be transformed to

$$-J\frac{\partial_x^* p}{\rho_0} = -gJ\frac{\rho(\zeta)}{\rho_0}\partial_x^*\zeta + J\int_\gamma^0 J(\partial_x b + \partial_x^*\gamma\partial_\gamma b)\,\mathrm{d}\gamma'. \tag{26}$$

The kinematic boundary conditions (7) and (8) are, under consideration of the transformed vertical velocity $\tilde{\omega}$, of simple form and therefore show a major advantage of generalised boundary-fitted vertical co-ordinates:

$$\tilde{\omega} = 0, \quad \gamma = -1, \tag{27}$$

$$\tilde{\omega} = 0, \quad \gamma = 0. \tag{28}$$

The concentration equation (10) reads in the transformed space as

$$\partial_t(Jc) + \partial_x(Juc) + \partial_y(Jvc) + \partial_\gamma(J\tilde{\omega}c) = 0. \tag{29}$$

By combining (14), (20), (22) and (23), a conservative formulation for the recalculation of the physical vertical velocity ω can be obtained:[11]

$$w = \frac{1}{J}(\partial_t(Jz) + \partial_x(Juz) + \partial_y(Jvz) + \partial_\gamma(J\tilde{\omega}z)). \tag{30}$$

It should be noted that w is not included in the transformed equations and therefore needs only to be evaluated for postprocessing reasons.

The well-known σ-co-ordinates introduced by Phillips[16] are the simplest special case of general vertical co-ordinates. They are based on the linear transformation function

$$\sigma = \frac{z-\zeta}{D}, \tag{31}$$

$$z = \sigma D + \zeta. \tag{32}$$

This results in $J = D$ for σ-co-ordinate models.

Another useful co-ordinate transformation is achieved by demanding that all vertical velocities vanish, i.e. $J\tilde{\omega} = 0$. Inserting this into the continuity equation (23) yields, after integrating it vertically from -1 to γ,

$$\partial_t z = -\partial_x\int_{-1}^{\gamma} Ju\,\mathrm{d}\gamma' - \partial_y\int_{-1}^{\gamma} Jv\,\mathrm{d}\gamma'. \tag{33}$$

This provides isopycnal co-ordinates with $\rho = \rho(\gamma)$ if the co-ordinate surfaces are initially isopycnal and no vertical mixing of density is assumed. This co-ordinate transformation which depends on the internal flow dynamics is not generally defined, because the monotonicity of $\gamma = \gamma(z)$ is not guaranteed. Furthermore, it is unstable if the vertical density stratification is too weak. However, combining this with other transformations seems to be promising (see Section 7.2).

4. LAYER INTEGRATION

As preparation for the discretization the transformed space (see Figure 1) is divided into N layers. Let

$$-1 = \gamma_0 = \cdots = \gamma_{\tilde{N}-1}(x,y) < \gamma_{\tilde{N}}(x,y) < \cdots < \gamma_N = 0 \tag{34}$$

for each position (x, y) be partitions of the interval $[-1, 0]$ and

$$\Delta\gamma_k(x,y) = \gamma_k(x,y) - \gamma_{k-1}(x,y) \tag{35}$$

for $1 \leqslant k \leqslant N$. In order to include step bottom hybrid models (see Section 6.2) in this theory, the layer interfaces γ_k may be functions of the horizontal position (x, y) but not of the time t. Here $\tilde{N}(x, y)$ denotes the lowest layer index with $\Delta\gamma_k(x, y) > 0$ for a given position (x, y). In most applications, e.g. in σ-co-ordinate models, $\tilde{N} = 1$ and γ_k are constant for all positions (x, y).

The integration of the continuity equation (23) over the kth layer reads, under consideration of the Leibniz rule

$$\int_{\gamma_{k-1}}^{\gamma_k} \partial_x f \, \mathrm{d}\gamma = \partial_x \int_{\gamma_{k-1}}^{\gamma_k} f \, \mathrm{d}\gamma - f(\gamma_k)\partial_x\gamma_k + f(\gamma_{k-1})\partial_x\gamma_{k-1}, \tag{36}$$

as

$$\begin{aligned}\partial_t \int_{\gamma_{k-1}}^{\gamma_k} J \, \mathrm{d}\gamma + \partial_x \int_{\gamma_{k-1}}^{\gamma_k} Ju \, \mathrm{d}\gamma + \partial_y \int_{\gamma_{k-1}}^{\gamma_k} Jv \, \mathrm{d}\gamma + (J\tilde{\omega} - Ju\partial_x\gamma - Jv\partial_y\gamma)_{\gamma=\gamma_k} \\ - (J\tilde{\omega} - Ju\partial_x\gamma - Jv\partial_y\gamma)_{\gamma=\gamma_{k-1}} = 0.\end{aligned} \tag{37}$$

With the definitions

$$h_k := \int_{\gamma_{k-1}}^{\gamma_k} J \, \mathrm{d}\gamma, \tag{38}$$

$$p_k := \int_{\gamma_{k-1}}^{\gamma_k} Ju \, \mathrm{d}\gamma, \qquad q_k := \int_{\gamma_{k-1}}^{\gamma_k} Jv \, \mathrm{d}\gamma, \tag{39}$$

$$u_k := \frac{p_k}{h_k}, \qquad v_k := \frac{q_k}{h_k}, \tag{40}$$

$$c_k := \int_{\gamma_{k-1}}^{\gamma_k} Jc \, \mathrm{d}\gamma, \qquad b_k := \int_{\gamma_{k-1}}^{\gamma_k} Jb \, \mathrm{d}\gamma, \tag{41}$$

$$\bar{w}_k := (J\tilde{\omega} - Ju\partial_x\gamma - Jv\partial_y\gamma)_{\gamma=\gamma_k}, \tag{42}$$

equation (37) can be rewritten as

$$\partial_t h_k + \partial_x p_k + \partial_y q_k + w_k - \bar{w}_{k-1} = 0. \tag{43}$$

Here we assume that the horizontal velocities are constant over the layer thickness. After this the layer-integrated momentum equations read as

$$\partial_t p_k + \partial_x(u_k p_k) + \partial_y(v_k p_k) + (\bar{w}_k u)_k - (\bar{w}_{k-1}u)_{k-1} - \tau_k^x + \tau_{k-1}^x + f q_k = P_k^x, \tag{44}$$

$$\partial_t q_k + \partial_x(u_k q_k) + \partial_y(v_k q_k) + (\bar{w}_k v)_k - (\bar{w}_{k-1}v)_{k-1} - \tau_k^y + \tau_{k-1}^y - f p_k = P_k^y, \tag{45}$$

with the shear stress

$$\tau_k^x = \left(\frac{\nu_t}{J}\partial_\gamma u\right)_k = (\nu_t \partial_z^* u)_k \tag{46}$$

and the layer-integrated pressure force

$$P_k^x = -\frac{1}{\rho_0}\int_{\gamma_{k-1}}^{\gamma_k} J\partial_x^* p \, \mathrm{d}\gamma. \tag{47}$$

The definitions for P_k^y and τ_k^y are analogous.

The layer integration of the pressure gradient force can be done in the following way:

$$\begin{aligned} P_k^x &= -gh_k\frac{\rho(\zeta)}{\rho_0}\partial_x^*\zeta + \int_{z_{k-1}}^{z_k}\int_z^{\zeta} \partial_x^* b \, \mathrm{d}z' \, \mathrm{d}z'' \\ &= -gh_k\frac{\rho()}{\rho_0}\partial_x^*\zeta + h_k\int_{z_k}^{\zeta} \partial_x^* b \, \mathrm{d}z' + \int_{z_{k-1}}^{z_k}(z'-z_{k-1})\partial_x^* b \, \mathrm{d}z' \\ &\approx -gh_k\frac{\rho(\zeta)}{\rho_0}\partial_x^*\zeta + h_k\left(\tfrac{1}{2}h_N(\partial_x^* b)_N + \sum_{j=k}^{N-1}\tfrac{1}{2}(h_j + h_{j+1})(\partial_x^* b)_j\right), \end{aligned} \tag{48}$$

with $z_k = z(\gamma_k)$ and

$$(\partial_x^* b)_k = \tfrac{1}{2}(\partial_x b_{k+1} + \partial_x b_k) - \partial_x z_k \frac{b_{k+1} - b_k}{\tfrac{1}{2}(h_{k+1} + h_k).} \tag{49}$$

The main approximation applied here was

$$\int_{z_{k-1}}^{z_k}(z'-z_{k-1})\partial_x^* b \, \mathrm{d}z' \sim \tfrac{1}{2}h_k^2(\partial_x^* b)_k. \tag{50}$$

The layer integration was carried out like this in order to achieve the exact value for the pressure gradient force when isopycnal co-ordinates are used, i.e. when $\partial_x b_k = 0$. Assuming a zero external pressure gradient and a two-layered flow with

$$\rho_k = \begin{cases} \rho_1 & \text{for } k > c, \\ \rho_2 & \text{for } k \leqslant c, \end{cases} \tag{51}$$

with $1 < c < N$, where the density interface z_c is a co-ordinate surface, the pressure gradient force would have the form

$$P_k^x = \begin{cases} 0 & \text{for } k > c, \\ -h_k\partial_x z_c g(\rho_2 - \rho_1)/\rho_0 & \text{for } k \geqslant c. \end{cases} \tag{52}$$

This gives the analytically correct form for the pressure gradient force as the product of the isopycnal slope and the reduced gravity.

We obtain (again approximating the horizontal advection terms) the following expression for the density equation:

$$\partial_t(h_k c_k) + \partial_x(p_k c_k) + \partial_y(q_k c_k) + (\bar{w}_k c)_k - (\bar{w}_{k-1} c)_{k-1} = 0. \tag{53}$$

It should be noted here that the governing equations (43)–(45) and (53) no longer contain the Jacobian J or the layer distribution in the transformed space γ. It is only necessary to compute the layer distribution in the physical space h_k. Another method for the derivation of these layer-integrated equations is to prescribe a time-dependent layer distribution in the physical space and then to integrate the equations over these layers under consideration of the Leibniz rule (36) (see e.g. Reference 17).

5. DISCRETIZATION

For the discretization the domain is horizontally divided into equidistant spatial increments Δx and Δy; the corresponding horizontal indices are i and j. The constant time step will be denoted by Δt. The notation for the discrete variables in the resulting staggered C-grid is shown in Figure 2. The local layer thicknesses at the u-, v- and c-points will be denoted by $h^u_{i,j,k}$, $h^v_{i,j,k}$ and $h^c_{i,j,k}$ respectively. Throughout this section, superscripts u, v and c indicate whether a u-velocity point, a v-velocity point or a concentration point is considered. The general time-stepping procedure will not be discussed here extensively. The free surface and the vertical diffusion are treated implicitly, all other terms explicitly. Two of the terms in the momentum equation, i.e. the horizontal momentum advection and the internal pressure gradient, will be discussed more thoroughly because their discretization may cause specific problems in general co-ordinates. For simplicity this discussion is based on situations with homogeneity in the y-direction.

5.1. Momentum advection

The discretization of the horizontal momentum advection is problematic in cases where the numerical grid is distorted, i.e. when a transformation other than the σ-transformation is used. Neglecting friction, diffusion, rotation and the pressure gradient, the 2D advection equation for momentum (1) reads as

$$\partial^*_t u + \partial^*_x u^2 + \partial_z(wu) = 0. \tag{54}$$

Assuming $u = u(t, x)$ is a function of time and horizontal position only, (54) can be rewritten by means of the continuity equation as

$$\partial^*_t u + \tfrac{1}{2}\partial^*_x u^2 = 0. \tag{55}$$

After initializing (54) with the vertically homogeneous u-profiles, the horizontal velocity will remain vertically homogeneous.

The discretization of the horizontal momentum advection in general co-ordinates should maintain this property. Otherwise, numerically induced vertical shear could lead to errors, especially in the

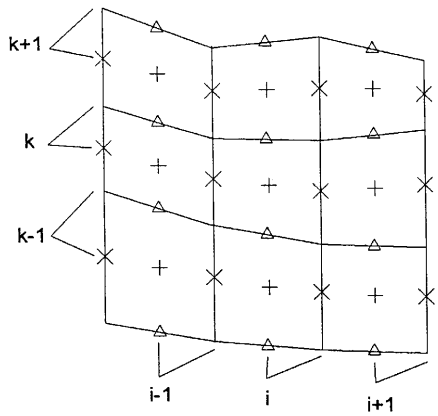

Figure 2. Sketch of vertical grid with indication of indexing: +, concentrations; ×, horizontal velocities; Δ, vertical velocities

turbulence modelling. In general co-ordinates the layer-integrated form of the 2D momentum advection equation reads as (see (44))

$$\partial_t(h_k u_k) + \partial_x(h_k u_k u_k) + (wu)_k - (wu)_{k-1} = 0. \tag{56}$$

A general, forward-in-time discretization of (56) has the form

$$\frac{\hat{h}^u_{i,k}\hat{u}_{i,k} - h^u_{i,k}u_{i,k}}{\Delta t} + A_{i,k} + \tfrac{1}{2}(w_{i+1,k} + w_{i,k})\bar{u}_{i,k} - \tfrac{1}{2}(w_{i+1,k-1} + w_{i,k-1})\bar{u}_{i,k-1} = 0, \tag{57}$$

where $A_{i,k}$ denotes the discrete horizontal advection term. With

$$A_{i,k} = \frac{(p_{i+1,k} + p_{i,k})\tilde{u}_{i+1,k} - (p_{i,k} + p_{i-1,k})\tilde{u}_{i,k}}{2\Delta x} \tag{58}$$

a momentum-conserving discretization of the horizontal advection can be achieved. In (57) and (58), $\tilde{u}_{i,k}$ and $\bar{u}_{i,k}$ are discrete velocity values which are taken into account for the horizontal and the vertical advection respectively. The determination of these advection velocities depends on the advection method chosen. Using central differencing, $\tilde{u}_{i,k} = \frac{1}{2}(u_{i,k} + u_{i+1,k})$ and $\bar{u}_{i,k} = \frac{1}{2}(u_{i,k} + u_{i,k-1})$ had to be chosen. A first-order upstream scheme would be achieved (in the case of $\tilde{u}_{i,k} > 0$ and $\frac{1}{2}(w_{i,k} + w_{i+1,k}) > 0$) with $\tilde{u}_{i,k} = u_{i,k}$ and $\bar{u}_{i,k} = u_{i,k}$.

The variables marked with a hat, $\hat{h}^u_{i,k}$ and $\hat{u}_{i,k}$, denote values on the new time level. For simplicity we assume that the water depth D^u_i is constant in time so that the local box heights do not vary in time, i.e. $\hat{h}^u_{i,k} = h^u_{i,k}$. For the momentum we write $p_{i,k} = h^u_{i,k}u_{i,k}$. If the velocities on the old time level, $u_{i,k}$, $\tilde{u}_{i,k}$ and $\bar{u}_{i,k}$, are vertically homogeneous, i.e. do not depend on the index k, it can be easily seen after eliminating the vertical velocities by using the discrete form of the continuity equation (43),

$$\frac{p_{i,k} - p_{i-1,k}}{\Delta x} + w_{i,k} - w_{i,k-1} = 0, \tag{59}$$

that the velocities on the new time level, $\hat{u}_{i,k}$, are only vertically homogeneous for local box heights which can be written as

$$h^u_{i,k} = \alpha_k D^u_i, \tag{60}$$

with $\alpha_k \geqslant 0$ and $\sum_{k=1}^{N} \alpha_k = 1$ and α_k not depending on the horizontal index i. This is only the case in σ-co-ordinates after equidistant or non-equidistant layer integration with constant values γ_k (see (34)). With all other co-ordinate transformations a numerically induced shear will be produced by advection of momentum.

This problem can be avoided if the horizontal advection term is discretized in a different way:

$$A_{i,k} = h^u_{i,k}u_{i,k}\frac{\tilde{u}_{i+1,k} - \tilde{u}_{i,k}}{\Delta x} + u_{i,k}\frac{p_{i+1,k} - p_{i-1,k}}{2\Delta x}. \tag{61}$$

Let $u_{i,k}$ again be vertically homogeneous, i.e. not depending on the index k. Now the second part of the discrete horizontal advection (61) cancels out with the vertical advection after being eliminated by means of the discrete continuity equation (59). In order to guarantee this, the same flux terms $p_{i,k}$ have to be used for the discrete continuity equation and the horizontal advection. Now $\hat{u}_{i,k}$ is independent of the vertical index k for all co-ordinate transformations.

The second part of (61) is a central discretization of a hyperbolic term which may lead to a higher instability of the scheme. As a compensation for that the first term will, in the numerical test shown later, be discretized upstream, which leads for $h^u_{i-1,k} = h^u_{i,k} = h^u_{i+1,k}$ and the Courant number $C = u_{i,k}\Delta t/\Delta x = \frac{1}{2}$ to the Lax–Wendroff scheme.

It is obvious that this new method is not momentum-conserving. Instead, a *conservation of homogeneous profiles* is guaranteed by this method. In the test cases considered here, the calculations

with σ-co-ordinates resulted in nearly identical results for both horizontal advection discretizations (see Section 7.1). However, the performance of the profile-conserving method should be proven in more complex situations.

It should be noted that this method guarantees exact profile conservation only if the free surface is not moving. For cases with significant temporal changes in water depth the exact profile conservation requires a more sophisticated discretization.

5.2. *Pressure gradient*

The internal part of the pressure gradient (48) will be discretized according to Mellor *et al.*[18] The crucial part of this term, which is $(\partial_x^* b)_k$ (in the case of the u-equation), is discretized between two vertically adjacent velocity points:

$$(\partial_x^* b)_k \sim \frac{\frac{1}{2}(b_{i+1,k+1} + b_{i+1,k}) - \frac{1}{2}(b_{i,k+1} + b_{i,k})}{\Delta x} - \partial_x z_k \frac{\frac{1}{2}(b_{i+1,k+1} + b_{i+1,k}) - \frac{1}{2}(b_{i+1,k} + b_{i,k})}{\frac{1}{2}(h^c_{i,k} + h^c_{i+1,k})}. \quad (62)$$

The discretization (62) can be written as

$$(\partial_x^* b)_k \sim \frac{(\frac{1}{2} - \alpha)b_{i+1,k+1} + (\frac{1}{2} + \alpha)b_{i+1,k} - (\frac{1}{2} + \alpha)b_{i,k+1} - (\frac{1}{2} - \alpha)b_{i,k}}{\Delta x}, \quad (63)$$

with $\alpha = \partial_x z_k \Delta x / (h^c_{i,k} + h^c_{i+1,k})$. For $|\alpha| \leqslant \frac{1}{2}$, (63) can be interpreted as interpolating vertically between $b_{i+1,k+1}$ and $b_{i+1,k}$ on one hand and between $b_{i,k+1}$ and $b_{i,k}$ on the other hand. For $|\alpha| > \frac{1}{2}$, extrapolations are made instead. The requirement $|\alpha| \leqslant \frac{1}{2}$ is commonly called the 'hydrostatic consistency condition' and can be written as

$$|\partial_x z_k| \frac{\Delta x}{\frac{1}{2}(h^c_{i,k} + h^c_{i+1,k})} \leqslant 1. \quad (64)$$

The two obvious ways to guarantee that (64) is fulfilled for a given co-ordinate transformation (fixed $\partial_x z$) are often unacceptable: thick layers could lead to an insufficient vertical resolution in the stratified region; a fine horizontal resolution could easily be computationally too expensive. The latter could, however, be afforded if unstructured grids in the horizontal are used, which are refined at locations with steep bottom slopes.

The problem with the hydrostatic consistency condition does not occur if the co-ordinate surfaces are horizontal ($\partial_x z_k = 0$) or coincide with isopycnals (surfaces of equal density), i.e. $\partial_x b_k = 0$. Considering the latter case by assuming the discrete equalities $b_{i+1,k+1} = b_{i+1,k}$ and $b_{i,k+1} = b_{i,k}$, (63) can be rewritten as

$$(\partial_x^* b)_k \sim -\partial_x z_k \frac{b_{i,k+1} - b_{i,k}}{\frac{1}{2}(h^c_{i,k} + h^c_{i+1,k})}. \quad (65)$$

This expression for all slopes $\partial_x z_k$, does not contain extrapolations and therefore does not lead to large errors.

It should be mentioned here that for the limit of the hydrostatic consistency condition, i.e. for $|\alpha| = \frac{1}{2}$, the numerator of (63) is simply the difference of two buoyancies. This leads to a relatively high accuracy for this specific situations (see also Reference 18).

6. HYBRIDIZATION TECHNIQUES

In this section, two hybrid transformations will be presented: the *mixed layer transformation* with a smooth bottom and the *z/σ-type transformation* with a step-like bottom. The first has a coarse and the latter a fine vertical resolution at the bottom.

6.1. Mixed layer transformation

This kind of transformation can be achieved by means of locally interpolating between an equidistant (in shallow water) and a non-equidistant (in deep water) discretization of the σ-transformation. This transformation will be referred to as the *mixed layer transformation*, because the co-ordinate surfaces will be concentrated near the surface. By doing this, an upper mixed layer could be highly resolved. Let $\beta(\sigma)$ be a non-equidistant discretization with σ from (31):

$$\beta(\sigma) = \frac{\tanh[d(1+\sigma)]}{\tanh(d)} - 1, \tag{66}$$

with $d > 0$ and $\gamma(\sigma)$ the mixed layer transformation

$$\gamma(\sigma) = \alpha\sigma + (1-\alpha)\beta(\sigma). \tag{67}$$

The local interpolation parameter α is calculated in such a way that the surface layer $h_N = -\gamma(\sigma_{N-1})D$, with $\sigma_{N-1} = -1/N$, always has the constant thickness $h_N = D_{\min}/N$:

$$\alpha = \min\left(\frac{(D_{\min}/D)\sigma_{N-1} - \beta(\sigma_{N-1})}{\sigma_{N-1} - \beta(\sigma_{N-1})}, 1\right). \tag{68}$$

Here $D_{\min}$ is a prescribed critical water depth. For shallow water with $D \leqslant D_{\min}$, equidistantly distributed σ-layers will be generated. It can happen that α becomes negative, which does not give problems in practical applications. The grid generated by the σ-transformation, which corresponds to the mixed layer transformation with the limit of $d \to 0$ in (66), is shown in Figure 3. The layer distributions for the mixed layer transformation with $d = 0{\cdot}5$ and 5 are shown in Figure 4. This method is easy to implement because it is based on a fixed number of vertical grid boxes of non-zero thickness.

6.2. z/σ-type transformation

The main task in introducing a step-like bottom co-ordinate is to determine the lower grid box indices $\tilde{N}^u_{i,j}$, $\tilde{N}^v_{i,j}$ and $\tilde{N}^c_{i,j}$ (once) and the vertical grid box heights $h^u_{i,j,k}$, $h^v_{i,j,k}$ and $h^c_{i,j,k}$ (in each time step) which always have to sum up to the actual water depth.

It is shown here how a hybridization can be achieved which allows for an arbitrary interpolation between a z-co-ordinate-type and a σ-co-ordinate model. We use the name z-co-ordinate-type model here in order to distinguish this from a z-co-ordinate model where the layers do not move with the free surface. Therefore such a z-co-ordinate-type model can in principle already be referred to as a hybrid z/σ-type model.

First the z-co-ordinate-type model will be constructed. Let $H_{\max}$ be the maximum water depth at a velocity point:

$$H_{\max} = \max_{i,j}(\max\{H^u_{i,j}, H^v_{i,j}\}). \tag{69}$$

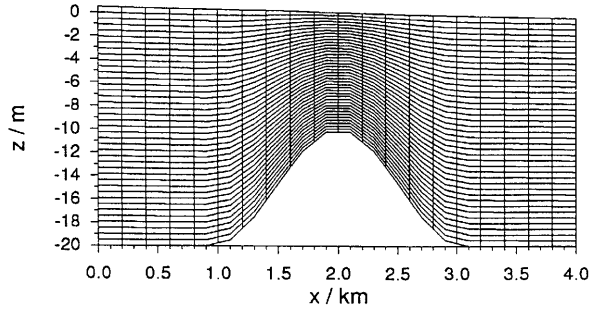

Figure 3. Grid with σ-transformation

Let Δz be a prescribed vertical increment (which will be the height of a grid box not disturbed by the bottom for $\zeta = 0$) and c, with $0 < c \leqslant 1$, a parameter which determines the minimum and the maximum grid box height at the bottom:

$$c\Delta z < h^u_{i,j,\tilde{N}^u_{i,j}} \leqslant (1+c)\Delta z, \qquad c\Delta z < h^v_{i,j,\tilde{N}^v_{i,j}} \leqslant (1+c)\Delta z. \tag{70}$$

Let

$$N = INT\left(\frac{H_{\max}}{\Delta z + 1 - c}\right) \tag{71}$$

be the number of vertical layers at the deepest point, where *INT* is the integer truncation function. We further define locally vertical increments $\Delta z^u_{i,j}$, $\Delta z^v_{i,j}$ and $\Delta z^c_{i,j}$ which in the case of the z-co-ordinate-

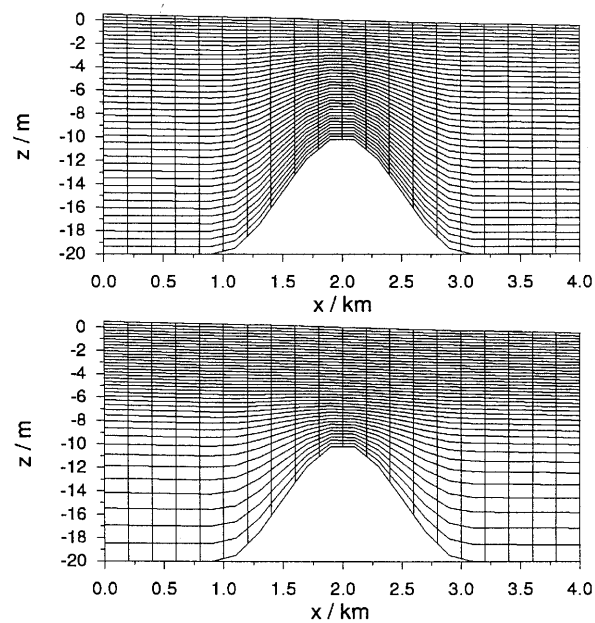

Figure 4. Two different realizations of mixed layer transformation (67) with $D_{min} = 10\,m$ (minimum water depth for undisturbed surface with $\zeta = 0$): upper panel, $d = 0{\cdot}5$; lower panel, $d = 5$

type model have (except in the bottom boxes) the value Δx. Now the bottom grid box indices at the velocity points can be defined as

$$\tilde{N}^u_{i,j} = N + 1 - INT\left(\frac{H^u_{i,k}}{\Delta z^u_{i,j}} + 1 - c\right), \tag{72}$$

$$\tilde{N}^u_{i,j} = N + 1 - INT\left(\frac{H^v_{i,k}}{\Delta z^v_{i,j}} + 1 - c\right). \tag{73}$$

The bottom grid box indices at the elevation points are calculated as

$$\tilde{N}^c_{i,j} = \min\{\tilde{N}^u_{i-1,j}, \tilde{N}^u_{i,j}, \tilde{N}^v_{i,j-1}, \tilde{N}^v_{i,j}\}. \tag{74}$$

The grid box heights at the velocity points are fitted to the actual water depth as

$$h^u_{i,j,k} = \begin{cases} \Delta z^u_{i,j} \dfrac{D^u_{i,j}}{H^u_{i,j}} & \text{for } \tilde{N}^u_{i,j} + 1 \leqslant k \leqslant N, \\ [H^u_{i,j} - (N - \tilde{N}^u_{i,j})\Delta z^u_{i,j}] \dfrac{D^u_{i,j}}{H^u_{i,j}} & \text{for } k = \tilde{N}^u_{i,j}, \end{cases} \tag{75}$$

$$h^v_{i,j,k} = \begin{cases} \Delta z^v_{i,j} \dfrac{D^v_{i,j}}{H^v_{i,j}} & \text{for } \tilde{N}^v_{i,j} + 1 \leqslant k \leqslant N, \\ [H^v_{i,j} - (N - \tilde{N}^v_{i,j})\Delta z^v_{i,j}] \dfrac{D^v_{i,j}}{H^v_{i,j}} & \text{for } k = \tilde{N}^v_{i,j}. \end{cases} \tag{76}$$

With

$$\tilde{M}^c_{i,j} = \max\{N^u_{i-1,j}, N^u_{i,j}, N^v_{i,j-1}, N^v_{i,j}\} \tag{77}$$

the grid box heights at the elevation points can be calculated as

$$h^c_{i,j,k} = \begin{cases} \Delta z^c_{i,j} \dfrac{D^c_{i,j}}{H^c_{i,j}} & \text{for } \tilde{M}^c_{i,j} + 1 \leqslant k \leqslant N, \\ \dfrac{[H^c_{i,j} - (N - \tilde{M}^c_{i,j})\Delta z^c_{i,j}] D^c_{i,j}/H^c_{i,j}}{\tilde{M}^c_{i,j} - \tilde{N}^c_{i,j} + 1} & \text{for } \tilde{N}^c_{i,j} \leqslant k \leqslant \tilde{M}^c_{i,j}. \end{cases} \tag{78}$$

This procedure guarantees that the grid box heights at one horizontal point always sum up to the local water depth.

The hybridization can now be easily applied. Let α be a parameter, $0 \leqslant \alpha \leqslant 1$. The local vertical increments will be an interpolation between the z-increments Δz and the σ-increments, which are determined as the local water depth divided by the number of layers, N:

$$\Delta z^u_{i,j} = \alpha \Delta z + (1 - \alpha)\frac{H^u_{i,j}}{N}, \tag{79}$$

$$\Delta z^v_{i,j} = \alpha \Delta z + (1 - \alpha)\frac{H^v_{i,j}}{N}, \tag{80}$$

$$\Delta z^c_{i,j} = \alpha \Delta z + (1 - \alpha)\frac{H^c_{i,j}}{N}. \tag{81}$$

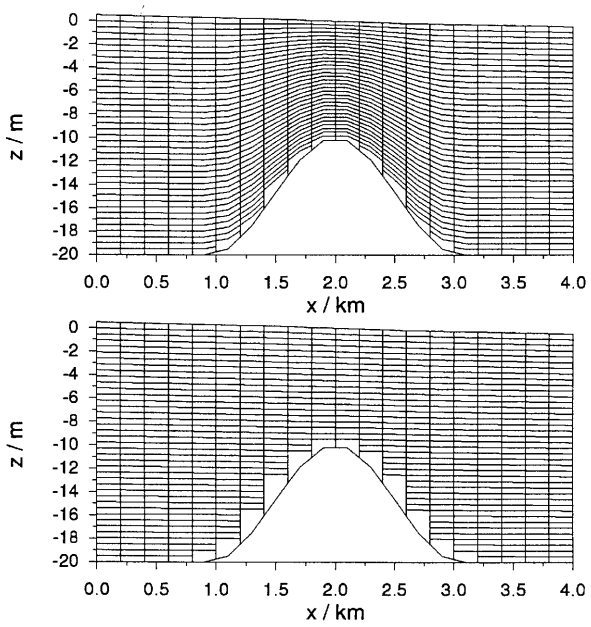

Figure 5. Two different realizations of z/σ-type transformation (79)–(81) with $c = 0{\cdot}5$ and $\Delta z = 0{\cdot}5$: upper panel, $\alpha = 0{\cdot}25$; lower panel, $\alpha = 1$

The following models are obtained: for $\alpha = 1$ the z-co-ordinate-type model (see Figure 5), for $\alpha = 0$ the σ-co-ordinate model (see Figure 3) and for other values between $\alpha = 0$ and 1 the *z/σ-type transformation* (see Figure 5).

The boxes with the concentrations $c_{i,j,k}$ with $\tilde{N}^c_{i,j} \leqslant k < \tilde{M}^c_{i,j}$ are considered as one box (see Figure 5) and are therefore mixed in a mass-conserving way after each time step. This is computationally more convenient than *a priori* treating these boxes as one. At velocity points adjacent to these boxes the co-ordinate slopes for the pressure gradients (62) are evaluated using one-sided differences.

7. 2D CHANNEL FLOW OVER A TOPOGRAPHIC BUMP

The performance of the different co-ordinate transformations will be tested on 2D barotropic and baroclinic flows over a topographic bump. For all test cases the same bathymetry will be used (see Figure 3–5), which was generated by the formula (values given in metres)

$$H = \begin{cases} 20 - 10\cos^2\left(\dfrac{x - 2000}{2000}\pi\right) & \text{for } 1000 \leqslant x \leqslant 3000, \\ 20 & \text{else.} \end{cases} \tag{82}$$

A large number of vertical layers ($N = 40$) are used in order to show how the violation of the hydrostatic consistency condition influences the results for the baroclinic calculations. In the horizontal, 20 increments with $\Delta x = 200\,\text{m}$ were used.

The parameterization of the bed friction was realized by using

$$\tau_b = \nu_t \partial_z u = r(\tilde{z}) u|u| \tag{83}$$

at the bottom, with the drag coefficient

$$r(\tilde{z}) = \frac{\kappa^2}{\ln^2(30\tilde{z}/K_s)}, \tag{84}$$

the von Kármn constant $\kappa = 0{\cdot}4$, the roughness length $K_s = 0{\cdot}1$ m and the distance from the bottom $\tilde{z} = K_s/30 + z + H$. This formulation for the bed friction is derived from assuming a logarithmic velocity profile near the bottom. It provides values for the bottom drag τ_b which are less sensitive to the distance from the bottom compared with values obtained via formulations with a constant drag coefficient r. This property is important when grids with strongly varying bottom box heights are used as in the z/σ-type model (see Figure 5). The internal friction has been parametrized by the parabolic profile

$$\nu_t = \kappa\tilde{z}\left(1 - \frac{\tilde{z}}{D}\right)|\tau_b|^{1/2}. \tag{85}$$

7.1. Barotropic flow

This barotropic flow case is mainly set up in order to test the profile-conserving momentum advection discretization discussed in Section 5.1. Here the σ-co-ordinate case (Figure 3) is compared with the z/σ-co-ordinate with $\alpha = 1$ (Figure 5), because the latter provides a significant violation of relation (60). The tests were run with and without friction. The barotropic forcing was imposed by an initial linearly sloping surface elevation with a difference of 0·01 m between the lateral ends of the channel. During the integration the surface elevation was fixed at the open boundaries. The time step was $\Delta t = 60$ s. The case without friction was integrated over $t = 4800$ s, the case with friction over $t = 12{,}000$ s.

An inspection of the resulting velocity profiles (see Figure 6) and the fluxes through the open boundary (see Table I) shows that the momentum-conserving advection discretization causes a strong acceleration of flow near the up-sloping bottom. In the case without friction the profile-conserving method provides vertically homogeneous profiles. This leads to a much better correlation between the σ-co-ordinate and z/σ-co-ordinate results also in the case with friction. The σ-co-ordinate results differed only insignificantly for both discretization methods. A comparison between the σ- and the mixed layer transformation where (60) is also violated showed similar results.

7.2. Two-layered flow

For the tests of the internal pressure gradient discretization a 2D two-layered flow over the topography given by (82) was set up. The densities were $\rho_1 = 1000\,\mathrm{kg\,m^{-3}}$ in the upper layer and $\rho_2 = 1020\,\mathrm{kg\,m^{-3}}$ in the lower layer. Mixing of density was excluded. Here the initial surface elevation was $\zeta = 0$, with fixed values at the open boundaries. The forcing was now imposed by an initially linearly sloping density interface ζ' with a mean position $z = -5$ m and a slope $\partial_x \zeta' = -5 \times 10^{-5}$. The density interface was fixed at the open boundaries. This test case was integrated over $t = 12$ h, when the flow was close to a steady state. The maximum internal Froude number was $Fr \approx 0{\cdot}15$.

A reference solution for this test case is calculated by using a partially isopycnal transformation. The density interface is considered as the co-ordinate surface with $k = N/2 = 20$, whereas the other

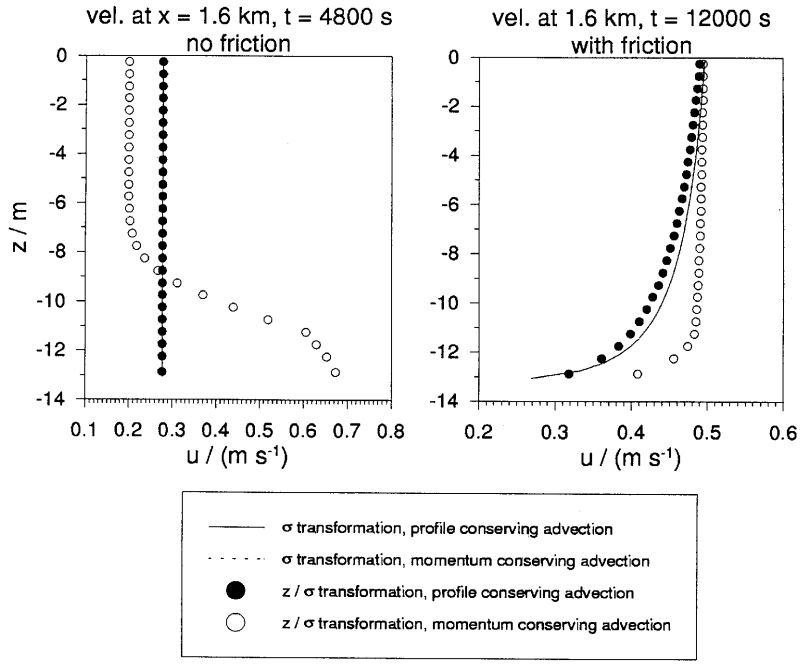

Figure 6. 2D barotropic open channel flow—velocity profiles at $x = 1{\cdot}6$ km calculated using σ- and σ/z co-ordinates with momentum-conserving and profile-conserving discretization of horizontal advection: left, without friction; right, with friction

co-ordinate surfaces are equidistantly distributed between the bottom and the interface and between the interface and the surface respectively. This is managed in the discrete space by integrating the continuity equation vertically from the bottom to the interface and then setting the vertical velocity at the interface to zero (see (33)).

Table I. Barotropic flow over bump: flux through open boundaries after $t = 4800$ s without friction and after $t = 12{,}000$ s with friction for different advection schemes and co-ordinate transformations. The relative flux error is given as $(F - F_0)/F_0$, where F_0 is the flux calculated with σ-co-ordinates and momentum-conserving advection. F_0 is $3{\cdot}68\,\mathrm{m^3\,s^{-1}}$ without friction and $6{\cdot}02\,\mathrm{m^3\,s^{-1}}$ with friction

Transformation	Advection	Friction	Flux error
σ	Mom.-cons.	No	0·0000
σ	Prof.-cons.	No	−0·0001
$\sigma/z, \alpha = 1$	Mom.-cons.	No	0·1199
$\sigma/z, \alpha = 1$	Prof.-cons.	No	−0·0001
σ	Mom.-cons.	Yes	0·0000
σ	Prof.-cons.	Yes	0·0004
$\sigma/z, \alpha = 1$	Mom.-cons.	Yes	0·0655
$\sigma/z, \alpha = 1$	Prof.-cons.	Yes	−0·0215

For running this test case with non-isopycnal co-ordinates, a routine for interpolating a density interface into a grid and detecting the interface in the grid afterwards has to be found. Here a conservative interpolation method is used:

$$\rho_{i,k} = \begin{cases} \rho_1 & \text{for } \zeta' \geqslant z_{i,k}, \\ \rho_2 & \text{for } \zeta' \leqslant z_{i,k-1}, \\ \dfrac{\zeta' - z_{i,k-1}}{h^c_{i,k}}\rho_1 + \dfrac{z_{i,k} - \zeta'}{h^c_{i,k}}\rho_2 & \text{else}, \end{cases} \tag{86}$$

where $z_{i,k}$ are the z-co-ordinates of the layer interfaces positioned a the w-points (see Figure 2). The time step for these calculations was $\Delta t = 20\,\mathrm{s}$ in order to stabilize the isopycnal solution. For the mass-conserving advection of density the fully two-dimensional uniformly third-order (in space) polynomial interpolation algorithm (UTOPIA) was implemented.[19] In order to have a monotone scheme, a multidimensional flux correction according to Zalesak[20] was applied. This computationally expensive discretization of the density advection was chosen in order to minimize problems connected with numerical diffusion and dispersion.

Besides with the σ- and isopycnal co-ordinates, this test case was also carried out with the z/σ-transformation ($\alpha = 0{\cdot}25, 0{\cdot}5, 1$) and mixed layer transformation ($d = 0{\cdot}5, 2, 5$). As an integral measure for comparing the eight methods under consideration, the vertically integrated flux through the open boundaries was calculated (see Table II).

An inspection of Table II shows that those co-ordinate transformations which provide horizontal co-ordinate surfaces in the area of the interface (σ/z-transformation with $\alpha = 1$ and the mixed layer transformation with $d = 5$). result in fluxes close to the flux calculated with the isopycnal co-ordinate. The more sloping the co-ordinate surface is in the vicinity of the interface, i.e. the larger the hydrostatic consistency criterion (see left side of relation (64)), the smaller the flux is. This is most extreme in the case of σ-co-ordinates.

Figures 7 and 8 show the interface position and the velocity profile at $x = 2{\cdot}4\,\mathrm{km}$ for the different co-ordinate transformations. The interface in the non-isopycnal models was defined as the vertical position with $\rho = \frac{1}{2}(\rho_1 + \rho_2)$, which was detected by means of (86). The plots of the velocity profiles confirm the results of Table II. Nevertheless, even for the mixed layer transformation with $d = 5$ and the z/σ-transformation with $\alpha = 1$ the interface positions behind the bump are higher than in the

Table II. Two-layered flow over bump: flux through open boundaries after $t = 12\,\mathrm{h}$ for different co-ordinate transformations. In the last column the hydrostatic consistency criterion (HCC, see left side of relation (64)) at $x = 2{\cdot}4\,\mathrm{km}$ and $z = -5\,\mathrm{m}$ is given. The relative flux error here was calculated as the relative deviation from the isopycnal solution, where the flux was $F_0 = 1{\cdot}52\,\mathrm{m^3\,s^{-1}}$

Co-ordinate transformation	Flux error	HCC
σ-transformation	−0·0890	2·14870
Isopycnal transformation	0·0000	—
σ/z-transformation, $\alpha = 0{\cdot}25$	−0·0488	1·39208
σ/z-transformation, $\alpha = 0{\cdot}5$	−0·0167	0·87775
σ/z-transformation, $\alpha = 1$	0·0070	0·00179
Mixed layer transformation, $d = 0{\cdot}5$	−0·0488	1·23785
Mixed layer transformation, $d = 2$	−0·0194	0·83847
Mixed layer transformation, $d = 5$	0·0090	0·10953

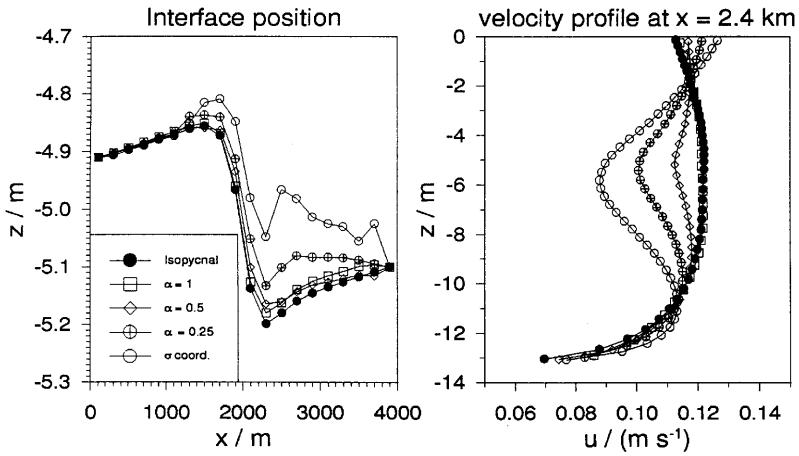

Figure 7. Two-layered flow over bump—interface position and velocity profile at $x = 2{\cdot}4$ km after $t = 12$ h: comparison between isopycnal transformation, z/σ-transformation for different α and σ-transformation

isopycnal reference solution. This could be caused by energy losses due to a small numerical diffusion still present in the density advection scheme.

The interface position and the velocity profile are far away from the reference solution for σ-coordinates. This is due to the violation of the hydrostatic consistency condition (64). However, even in cases where this condition is not violated, i.e. for the mixed layer transformation with $d = 2$ and the z/σ-transformation with $\alpha = 0{\cdot}5$, the resulting velocity profiles are disturbed.

The coarse bottom resolution for the mixed layer transformation with $d = 5$ and the steps at the bottom for the z/σ-transformation obviously do not lead to large errors. This might be due to the fact that the flow velocities are fairly small and also due to the use of the profile-conserving horizontal advection of momentum.

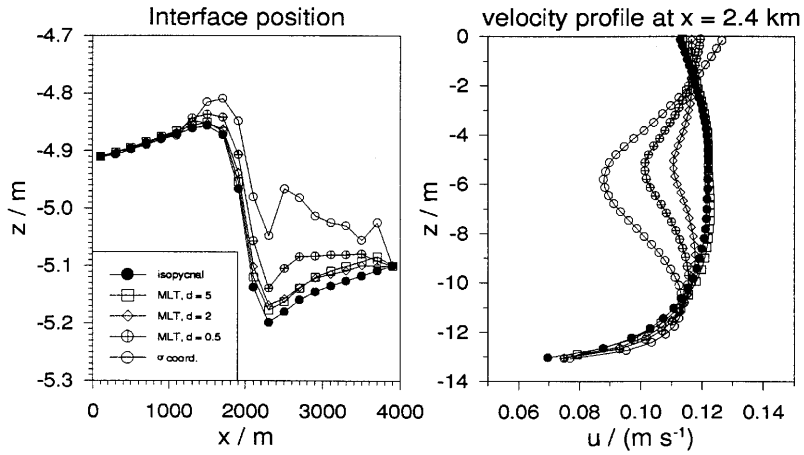

Figure 8. Two-layered flow over bump—interface position and velocity profile at $x = 2{\cdot}4$ km after $t = 12$ h: comparison between isopycnal transformation, mixed layer transformation for different d and σ-transformation

8. CONCLUSIONS

The barotropic experiments carried out in this paper showed that the discretization of horizontal advection has to be treated carefully in marine models with general vertical co-ordinates. Using the profile-conserving scheme rather than a momentum-conserving scheme significantly improved the performance of non-σ-co-ordinate models. This could be advantageous, especially in z-co-ordinate models, for coastal and estuarine applications where near-bottom advection plays an important role. However, in large-scale applications where momentum and potential vorticity conservation play a much more important role than near-bottom advection, the momentum-conserving advection probably gives better results that this new advection method.

It is shown with the two-layered flow experiment that the two-term formulation of the horizontal buoyancy gradient in general vertical co-ordinate models is problematic. In the case of moderately sloping isopycnals these two terms nearly cancel out analytically. After the discretization the error of the difference of these terms can be large, despite the fact that both terms have only relatively small truncation errors. It is shown that these errors can also be significant if the hydrostatic consistency condition is not violated. This problem does not occur in cases where one of the two terms is negligible. This is the reason why the results for the isopycnal co-ordinates on one hand and the z/σ-model with $\alpha = 1$ and the missed layer transformation with $d = 5$ on the other hand were so similar.

It can be concluded here that general co-ordinate models with an arbitrary layer distribution in the vertical can be advantageous compared with pure σ- or z-co-ordinate models. Once such a model is constructed, individual layer distribution rules can be defined which fit the vertical co-ordinate to the specific problem under consideration. This can include co-ordinate transformations that are much more sophisticated than those discussed in this paper.

ACKNOWLEDGEMENTS

This work was funded by the Danish Research Foundation, whose support is greatly appreciated. We further want to thank Julie Pietrzak and Hans Jacob Vested (Danish Hydraulic Institute), Tommy Jensen (Colorado State University) and Jean-Marie Beckers (Université de Liège, Belgium) for interesting discussions and helpful comments.

REFERENCES

1. R. L. Haney, 'On the pressure gradient force over steep topography in sigma coordinate ocean models,' *J. Phys. Oceanogr.*, **21** 610–619 (1991).
2. A. Beckmann and D. B. Haidvogel, 'Numerical simulation of flow around a tall isolated seamount. Part I: Problem formulation and model accuracy,' *J. Phys. Oceanogr.*, **23**, 1736–1753 (1993).
3. J. D. McCalpin, 'A comparison of second-order and fourth-order pressure gradient algorithm in a σ-co-ordinate ocean model,' *Int. j. numer. methods fluids*, **18**, 361–383 (1994).
4. G. S. Stelling and J. A. Th. M. van Kester, 'On the approximation of horizontal gradients in sigma co-ordinates for bathymetry with steep bottom slopes,' *Int. j. numer. methods fluids*, **18**, 915–935 (1994).
5. L. H. Slørdal, 'The pressure gradient force in sigma-coordinate ocean models,' *Int. j. numer. methods fluids*, **24**, 987–1017 (1997).
6. R. Bleck and L. T. Smith, 'A wind-driven isopycnic coordinate model of the North and Equatorial Atlantic Ocean. 1. Model development and supporting experiments', *J. Geophys. Res.*, **95**, 3273–3285 (1990).
7. K. Bryan, 'A numerical method for the study of the circulation of the world ocean', *J. Comput. Phys.*, **4** 347–376 (1969).
8. M. D. Cox, 'A primitive equation, 3-dimensional model of the ocean,' *GFDL Ocean Group Tech. Rep. 1*, Princeton University 1984.
9. V. Casulli and R. T. Cheng, 'Semi-implicit finite difference methods for three-dimensional shallow water flow,' *Int. j. numer. methods fluids*, **15**, 629–648 (1992).
10. H. Burchard, 'Turbulenzmodellierung mit Anwendungen auf thermische Deckschichten im Meer und Strömungen in Wattengebieten,' *Ph.D. Thesis GKSS 95/E/30*, University of Hamburg, GKSS Research Centre, 1995.

11. E. Deleersnijder and K. G. Ruddick, 'A generalized vertical coordinate for 3D marine problems,' *Bull. Soc. R. Sci. Liège*, **61**, 489–502 (1992).
12. C. W. Hirt, A. A. Amsden and J. L. Cook, 'An arbitrary Lagrangian–Eulerian computing method for all flow speeds,' *J. Comput. Phys.*, **14**, 227–253 (1974).
13. T. G. Jensen, 'A quasi-isopycnal upper ocean model for climate modelling,' *Proc. Fifth Symp. on Global Change Studies*, Nashville, TN, 1994, American Meteorological Society, 1997, pp. 77–80.
14. J. M. Beckers, 'Application of the GHER 3D general circulation model to the Western Mediterranean,' *J. Marine Syst.*, **1**, 315–332 (1991).
15. R. Gerdes, 'A primitive equation ocean circulation model using a general vertical coordiante transformation. 1. Description and testing of the model,' *J. Geophys. Res.*, **98** 14683–14701 (1993).
16. N. A. Phillips, 'A coordinate system having some special advantages for numerical forecasting,' *J. Meteorol.*, **14**, 184–185 (1957).
17. J. W. M. Lander, P. A. Blokland and J. M. de Kok, 'The three-dimensional shallow water model TRIWAQ with a flexible vertical grid definition,' National Institute for Coastal and Marine Management/RIKZ, *Workdocument RIKZ/OS-96.104x, SIMONA Rep. 96-01*, 1994.
18. G. L. Mellor, T. Ezer and L.-Y. Oey, 'The pressure gradient conundrum of sigma coordinate ocean models,' *J. Atmos. Oceanic Technol.*, **11**, 1126–1134 (1994).
19. B. P. Leonard, M. K. MacVean and A. P. Lock, 'The flux integral method for multidimensional convection and diffusion,' *Appl. Math. Model.*, **19** 333–342 (1995).
20. S. T. Zalesak, 'Fully multidimensional flux-corrected transport algorithms for fluids,' *J. Comput. Phys.*, **31**, 335–362 (1979).

